Intelligent Automation & Soft Computing
DOI: 10.32604/iasc.2023.031942
Article

Tech Science Press

Transformer Internal and Inrush Current Fault Detection Using Machine Learning

R. Vidhya[1,*], P. Vanaja Ranjan[2] and N. R. Shanker[3]

[1]Department of Electronics and Communication Engineering, Loyola-ICAM College of Engineering and Technology, Chennai, 600034, India
[2]Embedded System Technologies, Department of Electrical and Electronics Engineering, College of Engineering, Guindy, Chennai 600025, India
[3]Department of Computer Science and Engineering, Aalim Muhammed Salegh College of Engineering, Chennai 600055, India
*Corresponding Author: R. Vidhya. Email: vidhya.r@licet.ac.in
Received: 30 April 2022; Accepted: 07 June 2022

Abstract: Preventive maintenance in the transformer is performed through a differential relay protection system, and it protects the transformer from internal and external faults. However, the Current Transformer (CT) in the differential protection system mal-operates during inrush currents. CT saturates due to magnetizing inrush currents and causes false tripping of the differential relays. Moreover, identification of tripping in protection relay either due to inrush current or internal faults needs to be diagnosed. For the above problem, continuous monitoring of transformer breather and CT terminals with thermal camera helps detect the tripping in relay due to inrush or internal fault. The transformer's internal fault leads to high breathing process in the transformer breather, never for inrush currents. During inrush currents, CT temperature is increased. Continuous monitoring of breather and CT of the transformer through thermal imaging and radiometric pixels detect the causes of CT saturation and differentiates maloperation. Hybrid wavelet threshold image analytics (HWT-IA) based radiometric pixels analysis of the transformer breather and CT after de-noising provides an accurate result of about 95% for identification of the false tripping of differential protection system of transformer.

Keywords: Wavelet; threshold; inrush; transformer; breather; current transformer; thermal image

1 Introduction

The power transformer is an electrical device that works with an alternating current for long-distance power transmission. Transformers are used for several applications, such as increasing the voltage level of the secondary side output, distribution of power in industrial and residential areas, etc. The transformers require preventive and predictive maintenance to deliver an uninterrupted power supply. Faults in the transformers occur due to internal or external factors. Internal factors are composed of both electrical and mechanical faults. Electrical faults are due to winding failure and phase faults. Mechanical

faults occur due to the breakdown in the cooling medium's properties or while changing taps. Certain faults deteriorate the system with time causing insulation failure. In a transformer, oil is heated up to a high temperature in the internal part of the windings and causes the oil to expand, leading to a build-up of pressure in the conservator tank of the transformer. The transformer breather extracts moisture and dry air through the vent pipes of the conservator tank with silica gel crystals, which otherwise reduces the oil's dielectric strength [1]. The temperature of the surroundings below which the droplets of water start to condense leads to the formation of droplets in temperatures between −45°C to −25°C.

The breathing process intensifies during an overload or when an internal fault occurs since the rise of temperature in the conservator tank causes the oil to expand and contract faster. Under such conditions, the volume of air in-take increases which might eventually lead to early degradation of the silica gel crystals in the breather since there is comparatively a higher moisture ingress. Therefore, monitoring the temperature of the breather is also considered an essential step toward transformer maintenance. The protection system for the transformer is incorporated using differential relays [2]. The output of the current transformer is fed into the relay, where under normal conditions, the transformer primary and the secondary CTs generate the same amount of current on the secondary side of the CTs. Therefore, there is no net current flow in the differential relay. An internal fault or in-rush causes an imbalance in the output of these CTs, and there the net current flow causes the relay operating coil to trip and cuts off the transformer as a protection mechanism.

Furthermore, excessive differential currents between the primary and the secondary of the transformer affect transformer operation and differential protection relays that perform the protection task of the transformer. The relays mal operate when false differential currents occur during CT saturation [3]. Traditional CT current based analysis might be ineffective during saturated states. Mal-operation of differential protection system occurs during transients and inrush current. Magnetizing inrush, sympathetic inrush and external faults with current transformer (CT) saturation, capacitor switching, non-linear load switching, and Ferro resonance [4] are the causes of maloperation of CT in differential protection systems.

A higher magnitude of the second harmonic component present in the current waveform sampled by CT is generally used to differentiate inrush current from internal faults [5], but when the CT saturates, the amplitude of the second harmonic rises significantly and leads to misinterpretation in false tripping of the differential relays. CT saturation also leads to the blocking of harmonics, leading to the failure of most harmonics-based methodologies [6]. The differential current is analyzed using several techniques such as wavelet transformation and harmonic restraint method to prevent maloperation of the relay protection system and detect CT saturation level. In the analysis based on differential current, the algorithm highly depends upon the time to saturation of the CT and the number of sampling intervals of the normalized rotated differential current. Thereby discrepancies might occur in the results.

Hybrid Wavelet Thresholding based image analytics (HWT-IA) method for studying the false tripping of differential protection relay system due to internal faults and inrush current is proposed. Thermal image during tripping of differential protection system is analyzed based on CT saturation and different loading conditions and is used:

1. To differentiate internal fault and in-rush in the transformer during runtime, under various loads. Continuous monitoring through the thermal image of CT in normal and saturation conditions.
2. To detect tripping of differential protection relay system due to inrush or internal fault using the continuous monitoring of transformer breather and CT, through a thermal camera. Image analytics of acquired thermal images predict the reason for the tripping of the relay system.
3. To predict the reason for tripping of protection relay through thermal image analytics, which in prediction needs various data such as line voltage, load current, CT, room and breather temperature, humidity, On-load tap changer position etc.,

2 Literature Survey

Histogram analysis of the current signal is used for detection of maloperations in differential protection systems. Detecting the time difference between sudden changes occurring in the transformer wye-side current and differential current is proposed and avoids maloperation of transformer in substations. Degradation of transformer oil due to moisture ingress is protected through parallel plate capacitive moisture sensor fabrication in transformer breather and avoids moisture [7]. A transformer differential protection scheme is proposed to prevent false tripping due to CT saturation and fault detection modules based on differential wavelet transform of CT current signal. Three-phase differential currents are analyzed and used to differentiate the source of differential relay maloperation using a gradient boosting classifier. Higher-order statistics such as skewness and kurtosis discriminate between inrush current and internal faults in power transformers. A convolutional light-gated neural network-based composite learning structure is implemented to differentiate inrush current from internal faults of power transformers [8]. Conventional protection schemes based on phasor estimation are replaced by boundary wavelet coefficient energy for reliable discrimination between internal faults and inrush currents, a robust method in the presence of transients [9]. Condition monitoring is performed in distribution transformers by identifying the hot spot temperature of line joints, bushing etc., through thermal imaging methods [10]. Statistical features from the thermal images are used for fault detection in the transformer [11]. Transformer bushing faults are diagnosed using thermal images and a convolutional neural network [12]. Semi-supervised learning is performed using labelled and un-labelled image samples using the features such as temperature, shape and texture extracted from infra-red images of transformers for fault identification [13]. Thermal modelling and imaging are used to detect thermal faults in transformers based on the hot spot identification in the radiator and top oil [14]. Signal to noise ratio and mean square error of the transformer current output signal are improved by proposing modified soft and hard wavelet threshold functions [15].

A supervised machine learning approach considering wind speed and signal sampled from current transformers in wind farms to distinguish normal, internal and external faults is proposed [16]. Machine learning-based decision tree classifiers are listed to differentiate six types of transformer faults [17]. Machine learning-based extended Kalman filter hybridized with a support vector machine is used to classify faults that cause false tripping of differential protection system in three-phase transformers [18]. An exhaustive review of machine learning techniques is provided for electrical asset management and protection [19]. A differential protection scheme using a support vector machine is proposed and the accuracy achieved in detecting internal faults and inrush current is provided [20]. It is stated that probabilistic distance measures are often used in machine learning approaches, and it is apt for differentiating internal faults and inrush current in transformers [21].

3 Methodology

A 500 KVA, oil-cooled distribution transformer with a full load current of 666.68 A and 433 V on the low volt side is shown in Fig. 1 and the CT in Fig. 2. As per Fig. 3, the de-noised thermal images of the breather and current transformer differentiate the transformer's internal fault and inrush current. The transformer is continuously monitored with a thermal camera in the proposed method. Thermal image frames of the breather and current transformer captured simultaneously differentiate internal fault and inrush current. Whenever any internal fault occurs, the breather temperature increases, never for inrush current. The current transformer temperature increases during inrush current for a short period and internal faults in the transformer causes the current transformer temperature to increase rapidly. The differentiation of inrush and internal faults is performed by monitoring the thermal image frame of the breather and current transformer. However, correct prediction of inrush current requires a noise-free

thermal image for differentiation of inrush current levels and identification of the internal faults in the transformer.

Figure 1: Geotagged RGB image of transformer

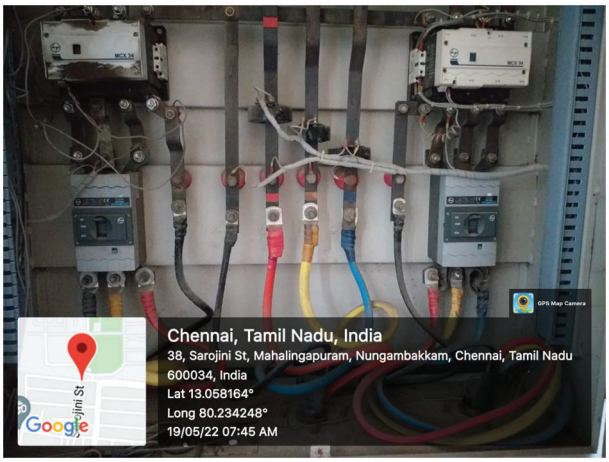

Figure 2: Geotagged RGB image of CT

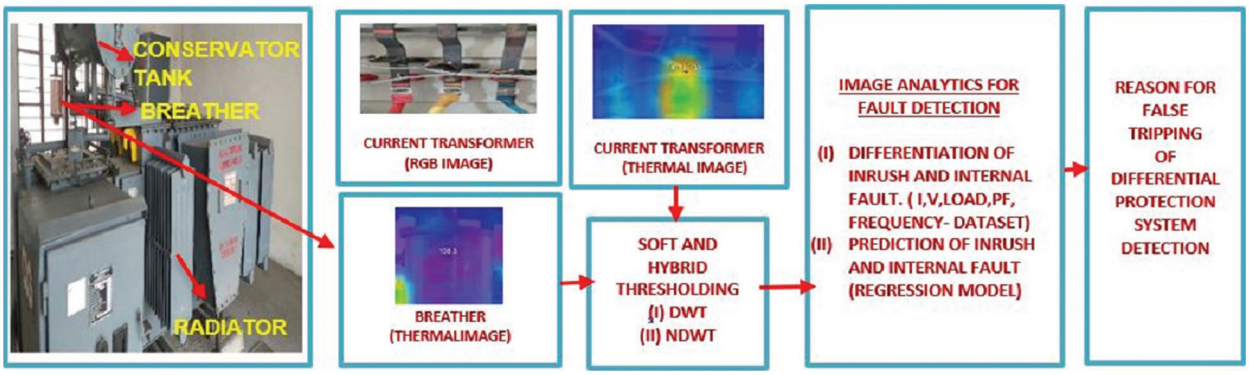

Figure 3: Block diagram for filtering the thermal images of breather and CT terminals

The thermal images of the breather and current transformer are acquired from a thermal camera and processed using Fluke SmartView software. The thresholding technique during discrete wavelet transform (DWT) de-noising plays a significant role in extracting the Region of Interest from the thermal images of the current transformer and breather. Moreover, DWT based adaptive thresholding is suitable for real-time applications. Ability to vary the threshold parameters is achieved by soft thresholding for removing noise. The residuals of the de-noised image at different decomposition levels are the target measurements, and hybridization of the thresholding techniques leads to improvised residuals in the de-noised image of the breather and CT terminal. Statistical parameters of the residuals of the decomposed image after wavelet transformation are considered for differentiation of inrush current and internal fault. The combination of wavelet transforms for hybrid thresholding discriminates the transformer breather image under fault conditions and the current transformer image during inrush current using a soft thresholding mechanism.

For the differentiation of the internal faults and inrush current, thermal images from the thermal camera are processed with different thresholding methods, and hybridization of thresholding leads to differentiation of the faults using statical pixel values.

In this paper, DWT based hybrid thresholding method is proposed. DWT is a frequency domain transformation technique where the process is initiated with a mother wavelet belonging to a family of wavelets such as Haar, Daubechies and Bior. The transformed image is a scaled and shifted version of the mother wavelet. The image is divided into sub-components named approximations that represent smoother sections of the image called low-frequency components and details; high-frequency components represent the edges in the image. The image is said to be decomposed when it is processed through successive low pass and high pass filters. After decomposition, thresholding is applied to enhance and de-noise the thermal images. In the proposed system, after DWT-based image decomposition, hybrid thresholding is applied for image enhancement.

Non-decimated DWT (NDWT) enhances the translation invariance by up-sampling the filter coefficients. NDWT is suitable for de-noising of images. The image's resolution is reduced by half at each level of discrete wavelet transform and never in NDWT. In NDWT, spatial resolution becomes coarse at higher levels while the size is retained as in DWT. In the proposed system, after NDWT decomposition of the image, hybrid thresholding is applied for image enhancement.

3.1 Thresholding and De-Noising of Thermal Images for Extraction of Operating Condition from Pixels

Wavelet transform smoothens the thermal image [22]. Wavelet is defined as in Eq. (1).

$$\psi_{a,b}(t) = \frac{1}{\sqrt{|a|}}\psi\left(\frac{t-b}{a}\right),\ a,\ b \in \mathrm{R},\ a \neq 0 \tag{1}$$

In Eq. (1), scaling parameter 'a' represents wavelet compression degree and translation parameter 'b' indicates the wavelet's location with respect to the time axis. If $|a| < 1$, then the wavelet is the compressed version of the mother wavelet and corresponds mainly to higher frequencies. When $|a| > 1$, the wavelet is an expanded version and corresponds to lower frequencies. Wavelet transform operates on the thermal image; the resultant coefficients represent noise with low energy, and the input image has a significant energy level. By applying proper thresholding, noises are removed. Effective noise removal algorithms preserve the edges and details in the image while removing the detrimental effects of noise and appropriately changing the transformation coefficients. Multi-level transforms are useful in information processing at successive levels, and edges become more prominent at each level.

Daubechies wavelet filter shows the scaling function and represents the greatest number of complex functions with few wavelet coefficients. Daubechies has a high degree of linearity in phase and smoothness in the decomposed image. Symlet filter is a modified form of the Daubechies wavelets, where

there is an inclination towards symmetry of the wavelets. Coiflet filters increase the pixel averaging, differencing computations and vanishes the moment property [23]. Biorthogonal wavelet filters are better suited for multiresolution analysis and extracting features of edges in the images rather than the orthogonal wavelet filters like Haar and Daubechies. They are realized using two different wavelets for decomposition and reconstruction and never to be orthogonal to each other. The reverse biorthogonal wavelet filter transform applies the synthesis and analysis scaling functions to the input image. Meyer wavelet filter is continuously differentiable and has a high probability of capturing events in a given window, indicative of compact support relating to time-localization. Fejer Korovkin wavelet filters exhibit more symmetry than Daubechies wavelets and compose the non-linear phase.

Thresholding plays a vital role in de-noising the decomposed images. The choice of an optimal threshold value is considered the major decision in the process. They are classified as soft and hard thresholding techniques where hard thresholding sets the wavelet decomposition coefficients to zero when the value is lesser than a specified threshold and retains the old value, if the value is greater than the threshold, as per Eq. (2).

$$\overline{\omega_{j,k}} = \begin{cases} \omega_{j,k}, & |\omega_{j,k}| \geq \lambda \\ 0, & |\omega_{j,k}| < \lambda \end{cases} \tag{2}$$

In soft thresholding, a part of the high-frequency decomposition coefficients is lost beyond the threshold.

$$\overline{\omega_{j,k}} = \begin{cases} \text{sgn}(\omega_{j,k})(|\omega_{j,k}| - \lambda), & |\omega_{j,k}| \geq \lambda \\ 0, & |\omega_{j,k}| < \lambda \end{cases} \tag{3}$$

In Eq. (3), Parameter $\overline{\omega_{j,k}}$ is the representation of estimated wavelet coefficients, parameter $\omega_{j,k}$ is the representation of the wavelet coefficients after decomposition, λ is the threshold, and sgn(*) is the symbolic piecewise function. The thresholding methods remove the un-scaled white noise present in the thermal image and differentiate the pixels for internal fault and inrush current. White noise generally has a constant value across the frequency spectrum. The pixels of the white noise in the thermal image have a uniform probability density function and are considered as independent random variables arranged in a rectangular grid in the thermal image. Humans can better differentiate between colours instead of gray levels; the advent of technology has led to colour thresholding, which provides more meaningful results and an enhanced image discrimination process. The original image captured using a visual IR thermometer and the corresponding thermal image of the breather and CT terminal are shown in Fig. 4.

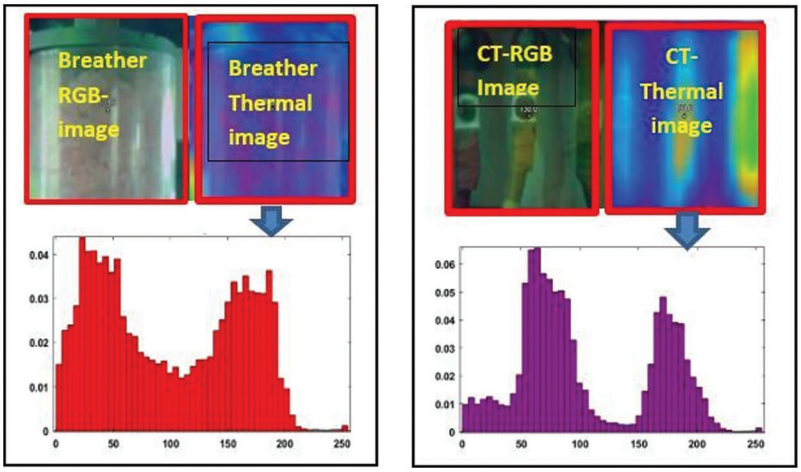

Figure 4: RGB and thermal images of breather and CT with histogram

The type of threshold to be adopted depends on the signal to noise ratio and the noise distribution. In the proposed work, un-scaled white noise in the thermal image is reduced. The thresholding function of hard type abruptly falls to zero when the image is identified with noise and never suits for roughness estimation. Penalize high, medium and low thresholding is of hard type, and soft thresholding can also be applied for temperature-based analysis. Soft type thresholding gradually reduces the magnitude of the transform coefficients beyond the threshold; for the values lesser than the threshold, the function falls to zero. The expected output image magnitude is lesser than the source and undesirable at certain times. The Soft type thresholding gives a smoother surface. The residuals of the de-noised thermal images at various decomposition levels, thresholding levels and histograms are analyzed with statistical values. The original thermal image, when processed by the wavelet filters, does not yield significant results, and the analysis appears to be normal, but the residuals from the decomposed image capture the variations based on the operating condition of the transformer in CT and Thermal images.

3.2 Sparsity Norm Based Soft Thresholding to Differentiate the Breather and CT Image for Fault Identification

Norm is a specific function used to measure the size of non-zero elements in a vector. It is an empirical method where the results are better verified through observation rather than relying on theoretical concepts. Three different methodologies followed for empirical implementation of thresholding strategies: Equal balance sparsity-norm, obtaining the square root of the threshold associated with Equal balance sparsity-norm or remove near 0. Sparsity implies that fewer number of large coefficients can optimally represent the information [24]. The repetition of a specific pattern characterizes wavelets. The notion of sparsity contradicts that of the density parameter. Sparsity dominates whenever there is a similarity in the area of focus. Sparsity is considered since there is a similarity in the periodic repetition of wavelets. The impact of sparsity plays a powerful role in the de-noised output image.

Balance sparsity norm thresholding of transformer breather thermal images produces a range of mean and standard deviation values for various wavelet transforms, and the best is observed for Daubechies wavelet level 3 decomposition, as shown in Tab. 1. The contribution of each pixel intensity is very high, and the edges are quite prominent in the denoised image. The mean value of the de-noised image residuals shows a sharp peak while using Daubechies (DB) wavelets for transformation, indicative of a significant change in the de-noised image at the third level of decomposition. No other wavelets show such variation when the decomposition levels are changed. Daubechies wavelet is used to de-noise breather thermal images, and it is further processed to differentiate the cause of protective system tripping that was either due to in-rush current or internal fault with CT saturation through thermal pixel values.

Table 1: Residuals of balance sparsity norm/soft thresholding of breather thermal images affected by unscaled white noise when there is an internal fault with CT saturation-(DWT)

Wavelet type/Level	Mean/Range	Mean absolute deviation	Standard deviation	L1 norm	L2 norm
Haar	$4 \times 10^{-2}/4$	16.6×10^{-2}	37.6×10^{-2}	$4.18e^{4}$	209.2
DB (10)/3	$\mathbf{18 \times 10^{-2}/18}$	$\mathbf{59.5 \times 10^{-2}}$	$\mathbf{85.4 \times 10^{-2}}$	$\mathbf{1.55e^{5}}$	**473.1**
Sym (8)/3	$10 \times 10^{-2}/10$	51×10^{-2}	81.7×10^{-2}	$1.56e^{5}$	453
Coif (5)/4	$12 \times 10^{-2}/12$	53.1×10^{-2}	83.8×10^{-2}	$1.62e^{5}$	464.3
Bior (6.8)/2	$9 \times 10^{-2}/10$	48.4×10^{-2}	71.9×10^{-2}	$1.21e^{5}$	398.7
Rbio (6.8)/3	$7 \times 10^{-2}/11$	49.5×10^{-2}	79.2×10^{-2}	$1.52e^{5}$	438.8
dmey/3	$11 \times 10^{-2}/13$	53.5×10^{-2}	85.4×10^{-2}	$1.63e^{5}$	473.2
fk (22)/4	$9 \times 10^{-2}/15$	53.96×10^{-2}	88.7×10^{-2}	$1.64e^{5}$	491.6

3.3 Fixed Form/Soft Thresholding of CT Terminal Images During Inrush Current Occurrence

The strategy suggested by the Donoho-Johnstone method is that when the noise ratio is small, then fixed form thresholding needs to be applied [25]. In this method, the deviation of noise samples at various instants from its mean value [mean absolute deviation] measured using the middle value in the data set of the coefficients under the different types of wavelet transforms is performed at various levels. The relative advantage of using fixed thresholding is that the image edges affect the image in certain conditions and, a fixed type of thresholding results in a comparatively lesser roughness value for the image. For 2D space, the fixed-form threshold T_F is defined as:

$$\boldsymbol{T_F = \sigma * \sqrt{2 * \log(r * c)}} \tag{4}$$

In Eq. (4), σ is the mean absolute deviation calculated at different decomposition levels and [r, c] is the surface gride size [26]. The obtained mean and standard deviation using fixed form thresholding as in Tab. 2 flattens from level 3 onwards for Haar, whereas for Biorthogonal wavelets, peak values of the contribution of pixels to the overall mean and a very prominent mean absolute deviation is observed for the third level of decomposition. Symlets, Discrete Meyer and Fejer-Korovkin wavelets yield no significant change in measured mean with respect to the transformation levels.

Table 2: Residuals of fixed form/soft thresholding of CT terminal thermal images affected by unscaled white noise during power-up [in-rush occurrence]–(NDWT)

Wavelet Type/Level	Mean/Range	Mean Absolute Deviation	Standard Deviation	L1 Norm	L2 Norm
Haar/1	$16 \times 10^{-2}/16$	23.13×10^{-2}	60.41×10^{-2}	$6.04e^{4}$	335.7
DB (10)/3	$35 \times 10^{-2}/59$	96.51×10^{-2}	1.973	$2.81e^{5}$	1094
Sym (8)/4	$38 \times 10^{-2}/38$	99.44×10^{-2}	1.678	$3.03e^{5}$	930.3
Coif (5)/2	$28 \times 10^{-2}/37$	56.9×10^{-2}	1.345	$1.72e^{5}$	745.6
Bior (6.8)/3	$\mathbf{50 \times 10^{-2}/50}$	**1.124**	**1.857**	$\mathbf{2.83e^{5}}$	**1029**
Rbio(6.8)/5	$15 \times 10^{-2}/35$	90.93×10^{-2}	1.47	$2.77e^{5}$	813.8
dmey/3	$25 \times 10^{-2}/55$	1.074	2.064	$3.24e^{5}$	1145
fk (22)/3	$47 \times 10^{-2}/57$	78.029×10^{-2}	2.141	$3.11e^{5}$	1187

The mean value of residuals of the de-noised image shows a sharp peak while using bi-orthogonal wavelets for transformation, which indicates a significant change in the de-noised image at the third level of decomposition. No other wavelets show such variation when the decomposition levels are changed. Therefore, bi-orthogonal wavelets can be used for de-noising CT terminal thermal images and the de-noised image can be further processed to differentiate the cause of protective system tripping that was either due to in-rush current or internal fault with CT saturation.

3.4 Fixed Form/Soft Thresholding of Breather Images During Internal Fault with CT Saturation

The mean value of residuals of the de-noised image never has a significant variation for any wavelet, as shown in Tab. 3. Decomposition never produces any deviations in the details produced from the image. The de-noised image will never be suitable for further processing to differentiate the cause of protective system tripping due to inrush current or internal fault with CT saturation.

Table 3: Residuals of fixed form/soft thresholding of breather thermal images affected by unscaled white noise when there is an internal fault with CT saturation-(DWT)

Wavelet type/Level	Mean/Range	Mean absolute deviation	Standard deviation	L1 Norm	L2 Norm
Haar/1	$2 \times 10^{-2}/2$	8.78×10^{-2}	26.6×10^{-2}	$2.18e^{4}$	147.8
DB (10)/1	$6 \times 10^{-2}/6$	18.8×10^{-2}	43.8×10^{-2}	$5.69e^{4}$	243.2
Sym (8)/5	$1 \times 10^{-2}/3$	23.5×10^{-2}	48.2×10^{-2}	$7.13e^{4}$	267
Coif (5)/3	$4 \times 10^{-2}/4$	23.03×10^{-2}	47.6×10^{-2}	$6.97e^{4}$	263.9
Bior (6.8)/3	$3 \times 10^{-2}/3$	22.2×10^{-2}	46.7×10^{-2}	$6.71e^{4}$	259
Rbio(6.8)/5	$4 \times 10^{-2}/4$	23.3×10^{-2}	47.9×10^{-2}	$7.04e^{4}$	265.4
dmey/5	$4 \times 10^{-2}/4$	23.1×10^{-2}	47.8×10^{-2}	$7.01e^{4}$	265
fk (22)/4	$4 \times 10^{-2}/4$	22.2×10^{-2}	47.03×10^{-2}	$6.78e^{4}$	260.7

3.5 Sparsity Norm/Soft Thresholding of CT Images Acquired During Inrush

The mean value of residual thermal images never significantly varied for different wavelet types, as shown in Tab. 4. Different decomposition levels never show any deviations in the thermal image. The de-noised thermal image can never be used to differentiate the source of protective system tripping, which arises due to an inrush current or internal fault in the transformer.

Table 4: Residuals of balance sparsity norm/Soft thresholding of CT thermal images affected by unscaled white noise when there is CT saturation during power-up [inrush occurrence]- NDWT

Wavelet type/Level	Mean/Range	Mean absolute deviation	Standard deviation	L1 Norm	L2 Norm
Haar/5	$26 \times 10^{-2}/6$	48.06×10^{-2}	53.2×10^{-2}	$8.06e^{4}$	295.1
DB (10)/1	$26 \times 10^{-2}/6$	58.8×10^{-2}	43.8×10^{-2}	$5.69e^{4}$	243.2
Sym (8)/4	$28 \times 10^{-2}/5$	35.2×10^{-2}	61.2×10^{-2}	$1.08e^{5}$	339
Coif (5)/4	$16 \times 10^{-2}/6$	34.5×10^{-2}	60.5×10^{-2}	$1.05e^{5}$	335.2
Bior (6.8)/5	$15 \times 10^{-2}/5$	33.9×10^{-2}	59.8×10^{-2}	$1.04e^{5}$	331.2
Rbio (6.8)/1	$29 \times 10^{-2}/4$	52.8×10^{-2}	42.1×10^{-2}	$5.4e^{4}$	233
dmey/5	$11 \times 10^{-2}/7$	34.91×10^{-2}	61.4×10^{-2}	$1.07e^{5}$	340.2
fk (22)/5	$21 \times 10^{-2}/7$	34.08×10^{-2}	61.14×10^{-2}	$1.05e^{5}$	338.9

3.6 Hybrid Thresholding Using Balance Sparsity Norm and Fixed Form

The hybrid wavelet threshold image analytics (HWT-IA) method is proposed by hybridizing the thresholding techniques such as balance sparsity norm and fixed form for de-noising CT and breather thermal images. The statistical values show significant changes in the mean and absolute deviation for a certain level of decomposition, and acquired thermal images show peaks of two different magnitudes in the residual mean value both during in-rush current occurrence using CT Terminal image and internal fault condition with CT saturation using breather image. Histogram peaks of thermal images show the differentiation of faults in the thermal images. The original and the enhanced images are shown in Fig. 5 and corresponding histograms in Fig. 6. The enhanced image's residual mean and absolute deviation value is as tabulated in Tab. 5.

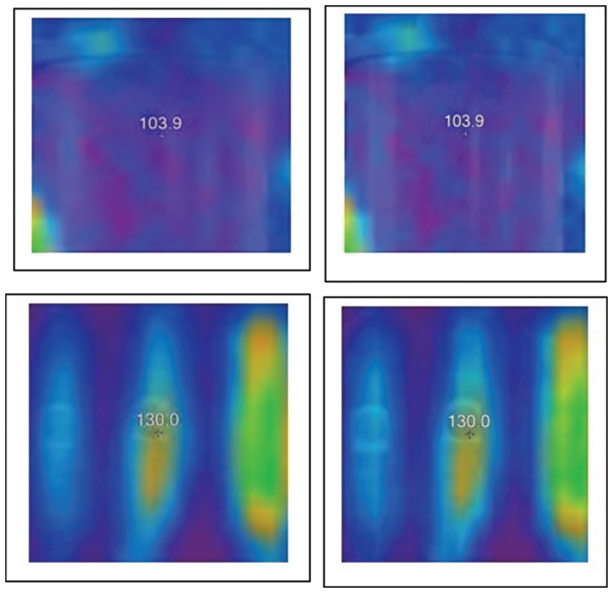

Figure 5: Top (left, right), Bottom (left, right) Original and enhanced image of transformer breather, CT terminals using hybrid thresholding (HWT-IA–NDWT)

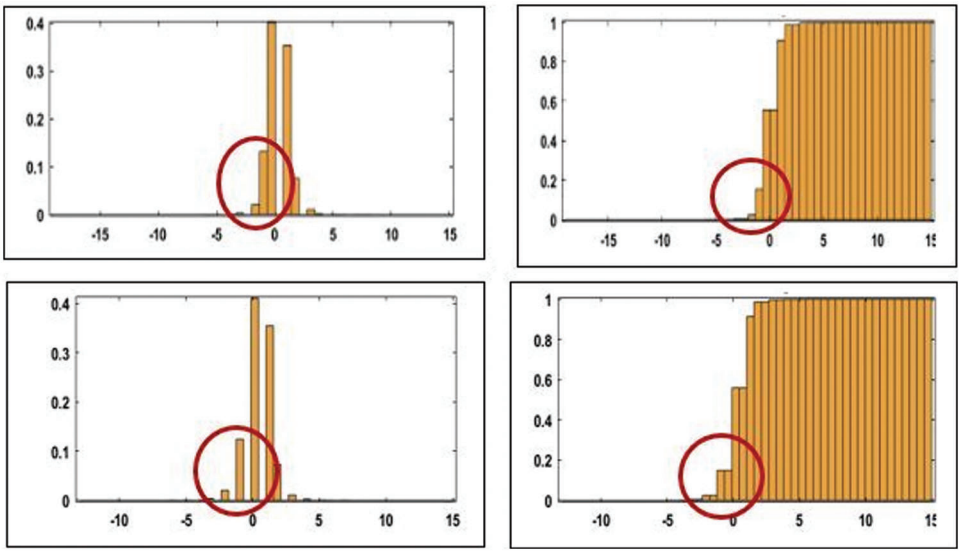

Figure 6: Top (left, right), Bottom (left, right) Histogram & cumulative histogram of residuals in the de-noised thermal image of breather and CT Terminals

Tab. 6 shows a set of data samples collected from transformers manufactured by Indo-Tech transformers, Palakkad and Current Electricals Ltd., Thirumudivakkam, to predict internal fault or inrush current faults. A thousand data samples were recorded from three different transformers in Loyola Campus, Nungambakkam, three from Nazareth college and four from Aalim Muhammed Salegh college of Engineering in Chennai, Tamil Nadu, India. These data are used for multiple regression modelling for the prediction of internal and inrush current faults

Table 5: Residuals of hybrid thresholding (HWT-IA) of breather [DWT] and CT terminal thermal images (NDWT) affected by unscaled white noise

Wavelet type/Level	Input image	Mean/Range	Mean absolute deviation	Standard deviation	L1 Norm	L2 Norm
DWT-(DB 10–level 3) (Balance sparsity norm and fixed form- HWT-IA)	Breather image (Internal fault with CT saturation]	$15 \times 10^{-2}/15$	47.5×10^{-2}	77.4×10^{-2}	$5.48e^{4}$	473.1
NDWT-(Bior 6.8–level 3) (Balance sparsity norm and fixed form- HWT-IA)	CT terminal [during inrush occurrence]	$48 \times 10^{-2}/48$	91.25×10^{-2}	1.751	$2.65e^{5}$	1015

3.7 Multiple Linear Regression

Explanatory variables, which include mean, standard deviation and entropy of the denoised images and the temperature values of the breather and current transformer under various conditions such as in-rush occurrence, fault and normal conditions, are considered for transformer fault prediction through multiple linear regression model. The model assumes that observations are chosen randomly from the existing database, and the distribution of residuals is normal with a mean value of zero. The r^2 value, which is the coefficient of determination, is about 86.68% for statistical parameters obtained due to continuous monitoring and thermal image analysis of the breather and current transformer acquired using a thermal camera. The *p*-value of 0.0007 indicates that the probability of the predictions varying from the null hypothesis, which implies that there is no correlation among the explanatory variables, is very less, and therefore the prediction made is relevant to the operating condition of the transformer. The residual standard error signifies the deviation of the prediction from the ideal fit, and the degrees of freedom depend on the difference between the sample size and the parameters used in the multiple linear regression model. β0–β8 represent the linear model coefficients, indicating the intercept and the slope. The representative parameters and the response variable are included in Tab. 7. Fig. 7 shows the histogram of residual and normal probability plot of residuals.

Eq. (5) shows the prediction equation of fault detection.

$$\begin{aligned} Operating\ Condition = &-10.1695 + 0.0397 \cdot Breather\ Mean - 0.006 \cdot Breather\ SD(Standard\ Deviation) \\ &+ 1.0828 \cdot Breather\ Entropy + 0.0249 \cdot CT\ Mean + 0.0024 \cdot CT\ SD \\ &- 0.8796 \cdot CT\ Entropy + 0.0016 \cdot Breather\ Temp + 0.0308 \cdot CT\ Temp \end{aligned} \tag{5}$$

The prediction accuracy of the proposed method (HWT-IA) and its characteristics are compared with that of light-gated recurrent unit (LGRU), gated recurrent unit (GRU), convolutional light-gated neural network (CLGNN) and conventional neural network (CNN) as shown in Tab. 8. The proposed method is based on image analytics employing a non-contact approach to create a real-time dataset, whereas the other techniques have utilized datasets acquired using invasive techniques. The above multiple linear regression equation for prediction, Eq. (5) is applied for the transformer dataset, and their results are shown in Tab. 9. The transformer condition is validated through created faults and CT [Current Transformer] signals.

Table 6: Data collection from transformers for prediction of internal fault or inrush current

Line Voltage	CT–I (Amps)	Hz	Cos φ	OLTC Tap Position	Load %	Breather image denoised mean value (DWT) & HWT-IA	Breather image denoised–SD (DWT) & HWT-IA	Breather denoised entropy (DWT) & HWT-IA	CT Image denoised mean value (NDWT) & HWT-IA	CT image denoised–SD (NDWT) & HWT-IA	CT denoised entropy (NDWT) & HWT-IA	Breather temp	CT Temp	Condition	Operating condition	Error	Accuracy
236.5	216.6	50.0	0.99	9	20.5	119.1	67.0	7.36	108.0	79.0	7.75	131.4	123.8	**Fault**	**2**	0.457	**77.16**
236.4	1604.8	50.0	1	10	28.4	88.5	58.7	7.42	137.2	80.0	7.81	123.1	153.3	Inrush	3	0.006	**99.81**
233.9	87.4	50.0	1	5	12.3	97.1	62.6	7.12	100.9	60.3	7.28	112.9	120.7	Normal	1	0.413	**58.68**
236.7	252.0	50.0	1	4	23.9	119.1	61.9	7.21	103.9	63.3	7.51	144.9	114.9	**Fault**	**2**	0.129	**93.54**
237.2	5910.0	50.0	0.98	11	42.0	88.5	61.9	7.13	142.0	60.9	7.76	117.7	185.5	Inrush	3	0.828	**72.40**
237.6	4304.4	50.0	1	8	36.1	90.0	63.7	7.14	127.7	61.5	7.58	114.4	180.7	Inrush	3	0.518	**82.74**
239.0	3541.5	50.0	0.98	7	33.9	97.2	56.9	7.28	117.6	62.3	7.54	116.3	175.6	Inrush	3	0.624	**79.19**
235.2	4923.0	50.1	0.97	0	38.6	87.0	62.9	7.03	137.5	57.8	7.66	104.9	182.6	Inrush	3	0.498	**83.40**
236.2	2917.2	49.9	0.98	4	31.8	96.7	59.6	7.08	117.8	58.0	7.53	109.8	164.0	Inrush	3	0.014	**99.54**
235.0	162.6	50.0	1	4	15.3	110.3	61.8	7.25	104.3	80.0	7.52	117.8	119.9	**Fault**	**2**	0.020	**99.02**
233.9	55.9	50.0	1	5	7.8	94.6	60.2	7.41	101.5	60.5	7.51	103.0	107.7	Normal	1	0.011	**98.94**
236.5	2346.3	50.0	0.96	9	30.3	90.7	61.2	7.16	114.9	57.6	7.41	107.5	156.1	Inrush	3	0.411	**86.31**
239.7	92.9	50.0	1	0	13.4	94.9	61.0	7.24	113.2	58.9	7.49	105.6	123.7	Normal	1	0.674	**32.58**
240.8	100.4	50.0	0.99	0	14.5	95.8	62.0	7.28	102.5	81.8	7.32	109.6	118.3	Normal	1	0.509	**49.12**
240.0	282.8	50.1	0.98	0	27.1	118.2	89.1	7.24	104.0	80.9	7.67	138.2	121.9	**Fault**	**2**	0.092	**95.39**
233.6	71.8	50.1	1	5	10.1	94.8	62.4	7.42	105.2	61.1	7.43	106.8	120.0	Normal	1	0.600	**39.98**
239.9	117.4	50.0	1	9	16.9	94.1	55.7	7.29	103.0	58.7	7.48	110.2	111.2	Normal	1	0.072	**92.79**
237.3	1880.1	49.9	0.98	0	29.7	90.0	61.3	7.33	128.6	59.0	7.66	101.3	154.6	Inrush	3	0.191	**93.63**
234.0	129.4	50.0	0.98	4	18.2	94.8	62.5	7.37	111.6	60.0	7.71	102.5	121.7	Normal	1	0.493	**50.69**
236.0	278.9	50.0	0.96	0	26.3	118.9	64.8	7.26	99.8	79.9	7.56	132.1	123.4	**Fault**	**2**	0.306	**84.68**

Table 7: Statistical parameters for denoised images of DWT and NDWT–(HWT-IA)

Predictor	Coefficient	Estimate	Standard error	t-statistic	*p*-value
Constant	β0	−10.1695	9.2609	−1.0981	0.2956
Breather Mean	β1	0.0397	0.0339	1.1718	0.266
Breather SD	β2	−0.006	0.0195	−0.3072	0.7644
Breather Entropy	β3	1.0828	1.5373	0.7043	0.4959
CT mean	β4	0.0249	0.0349	0.7135	0.4904
CT SD	β5	0.0024	0.0148	0.1603	0.8755
CT entropy	β6	−0.8796	1.8915	−0.465	0.651
Breather Temp	β7	0.0016	0.0185	0.0889	0.9308
CT temp	β8	0.0308	0.0094	3.26	0.0076

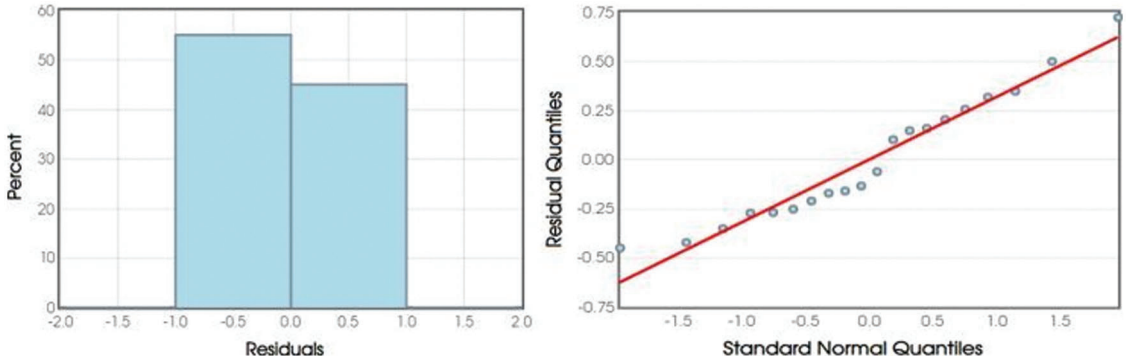

Figure 7: (Left, right) Histogram of residuals and normal probability plot of residuals

Table 8: Comparison of prediction accuracy

Classifier	Data acquisition technique	Prediction accuracy (%)
LGRU	Contact	98.59
GRU	Contact	98.37
CLGNN	Contact	99.63
CNN	Contact	98.44
HWT-IA	Non-contact	99.81

Table 9: Proposed HWT-IA using multiple regression applied on transformer dataset for accuracy in prediction

New transformer rating & company	Breather image denoised Mean Value (DWT) & HWT-IA	Breather image denoised–SD (DWT) & HWT-IA	Breather denoised entropy (DWT) & HWT-IA	CT image denoised mean value (NDWT) & HWT-IA	CT image denoised–SD (NDWT) & HWT-IA	CT denoised entropy (NDWT) & HWT-IA	Condition	Prediction
T1/500KVA/666.6 A, 433 V, Indo-Tech Transformers, Palakkad	118.5	66.0	7.48	110.0	81.0	7.71	Inter-turn fault	Correct
T2/800KVA/ 1066.69 A, 433 V, Current Electrical Ltd., Thirumudivakkam	86.3	51.7	7.38	142.2	79.0	7.84	Inrush	In-correct
T3/1000KVA/ 1333.51 A, 433 V, Current Electrical Ltd., Thirumudivakkam	91.1	61.9	7.19	99.9	63.3	7.31	Normal	Correct
T4/750KVA/ 1000.05 A, 433 V, Current Electrical Ltd., Thirumudivakkam	117.1	62.1	7.31	111.9	65.6	7.68	Core fault	Correct
T5/300KVA/417.37 A, 415 V, Current Electrical Ltd., Thirumudivakkam	85.5	61.9	7.18	148.0	60.9	7.79	Inrush	Correct
T5/300KVA/417.37 A, 415 V, Current Electrical Ltd., Thirumudivakkam	101.5	61.3	7.42	146.8	78.9	7.39	Transient fault	Correct

4 Conclusion

Automation of certain processes which otherwise require personnel for continuous monitoring has reduced the risk to human lives. Transformer breathers have silica gel that varies its colour to indicate the presence of moisture in the air intake for the transformer breathing mechanism. Visual inspection of the breather is required for the replacement of the gel. A novel hybrid thresholding methodology is proposed to differentiate the root cause of false tripping in the transformer's differential protection relay system and thus contributing to preventive maintenance of power and distribution transformers. The residuals of the de-noised thermal image of the breather in a distribution transformer are compared by applying wavelet transformation with a varied choice of wavelets. The maximum contribution of the intensity of each pixel towards the total image intensity in the de-noised thermal image of the breather was identified, and a modified form of thresholding is proposed by combining balance sparsity norm and fixed form thresholding to effectively remove the unscaled white noise in the thermal images of transformer breather and CT. Significant improvement in the mean and absolute deviation is observed in the stated residual parameters. The maximum prediction accuracy achieved is 99.81%, and the test data of five different live transformers from the operating field is applied to the model for prediction, where five out six predictions match the actual operating condition. The probability that the prediction varies from the null hypothesis prediction is 7×10^{-4}, which indicates that the image parameters analyzed are representative features of transformer operating condition. Fuzzy clustering and deep learning could be applied to the de-noised images to probe into transformer performance analysis under varying load conditions.

Acknowledgement: We thank the Managements of Loyola-ICAM College of Engineering and Technology (LICET), Loyola College, Loyola Institute of Business Administration (LIBA), Nazareth College and Aalim Muhammed Salegh college of Engineering for permitting us to utilize their facilities such as transformers to pursue the research work.

Funding Statement: The authors received no specific funding for this study.

Conflicts of Interest: The authors declare that they have no conflicts of interest to report regarding the present study.

References

[1] S. Kumar, L. Kumar, T. Islam and K. K. Raina, "Condition monitoring of transformer breather using a capacitive moisture sensor," *IEEE Transactions on Industrial Electronics*, vol. 67, no. 11, pp. 9779–9789, 2020.

[2] A. Ngaopitakkul and C. Jettanasen, "A discrete wavelet transform approach to discriminating among inrush current, external fault, and internal fault in power transformer using low-frequency components differential current only," *IEEJ Transactions on Electrical and Electronic Engineering*, vol. 9, no. 3, pp. 302–314, 2014.

[3] T. Zheng, J. Gu, S. F. Huang, F. Guo and V. Terzija, "A new algorithm to avoid maloperation of transformer differential protection in substations with an inner bridge connection," *IEEE Transactions on Power Delivery*, vol. 27, no. 3, pp. 1178–1185, 2012.

[4] P. K. Bera, C. Isik and V. Kumar, "Discrimination of internal faults and other transients in an interconnected system with power transformers and phase angle regulators," *IEEE Systems Journal*, vol. 15, no. 3, pp. 3450–3461, 2020.

[5] T. Zheng, T. Huang, Y. Ma, Z. Zhang and L. Liu, "Histogram-based method to avoid maloperation of transformer differential protection due to current-transformer saturation under external faults," *IEEE Transactions on Power Delivery*, vol. 33, no. 2, pp. 610–619, 2018.

[6] M. Stanbury and Z. Djekic, "The impact of current-transformer saturation on transformer differential protection," *IEEE Transactions on Power Delivery*, vol. 30, no. 3, pp. 1278–1287, 2015.

[7] L. Zhang, Q. H. Wu, T. Y. Ji and A. Q. Zhang, "Identification of inrush currents in power transformers based on higher-order statistics," *Electric Power Systems Research*, vol. 146, no. 2, pp. 161–169, 2017.

[8] S. Afrasiabi, M. Afrasiabi, B. Parang and M. Mohammadi, "Designing a composite deep learning based differential protection scheme of power transformers," *Applied Soft Computing Journal*, vol. 87, no. 1, pp. 231–243, 2020.

[9] R. P. Medeiros, F. B. Costa and K. M. Silva, "Power transformer differential protection using the boundary discrete wavelet transform," *IEEE Transactions on Power Delivery*, vol. 31, no. 5, pp. 2083–2095, 2016.

[10] T. Mariprasath and V. Kirubakaran, "A real time study on condition monitoring of distribution transformer using thermal imager," *Infrared Physics & Technology*, vol. 90, pp. 78–86, 2018.

[11] Z. A. Jaffery and A. K. Dubey, "Design of early fault detection technique for electrical assets using infrared thermograms," *International Journal of Electrical Power & Energy Systems*, vol. 63, pp. 753–759, 2014.

[12] J. Jiang, Y. Bie, J. Li, X. Yang, G. Ma *et al.,* "Fault diagnosis of the bushing infrared images based on mask R-CNN and improved PCNN joint algorithm," *High Voltage*, vol. 6, no.1, pp. 116–124, 2021.

[13] J. Fang, F. Yang, R. Tong, Q. Yu and X. Dai, "Fault diagnosis of electric transformers based on infrared image processing and semi-supervised learning," *Global Energy Interconnection*, vol. 4, no. 6, pp. 596–607, 2021.

[14] V. Shiravand, J. Faiz, M. H. Samimi and M. Mehrabi-Kermani, "Prediction of transformer fault in cooling system using combining advanced thermal model and thermography," *IET Generation, Transmission and Distribution*, vol. 15, no. 13, pp. 1972–1983, 2021.

[15] L. Jing-Yi, L. Hong, Y. Dong and Z. Yan-Sheng, "A new wavelet threshold function and denoising application," *Mathematical Problems in Engineering*, vol. 2, pp. 1–9, 2016.

[16] N. Rezaei, M. N. Uddin, I. K. Amin, M. L. Othman, M. B. Marsadek *et al.,* "A novel hybrid machine learning classifier-based digital differential protection scheme for intertie zone of large-scale centralized DFIG-based wind farms," *IEEE Transactions on Industry Applications*, vol. 56, no. 4, pp. 3453–3465, 2020.

[17] S. Ghosh and S. Dutta, "Ensemble machine learning methods for better dynamic assessment of transformer status," *Journal of the Institution of Engineers (India): Series B*, vol. 102, no. 5, pp. 1113–1122, 2021.

[18] Z. Kazemi, F. Naseri, M. Yazdi and E. Farjah, "An EKF-SVM machine learning-based approach for fault detection and classification in three-phase power transformers," *IET Science, Measurement and Technology*, vol. 15, no. 2, pp. 130–142, 2021.

[19] F. Aminifar, M. Abedini, T. Amraee, P. Jafarian, M. H. Samimi *et al.,* "A review of power system protection and asset management with machine learning techniques," *Energy Systems*, vol. 12, no. 3, pp. 1–38, 2021.

[20] L. D. Simões, H. J. D. Costa, M. N. O. Aires, R. P. Medeiros, F. B. Costa *et al.,* "A power transformer differential protection based on support vector machine and wavelet transform," *Electric Power Systems Research*, vol. 197, pp. 146–154, 2021.

[21] M. Tajdinian and H. Samet, "Application of probabilistic distance measures for inrush and internal fault currents discrimination in power transformer differential protection," *Electric Power Systems Research*, vol. 193, pp. 93–105, 2021.

[22] M. Sifuzzaman, M. Islam and M. Ali, "Application of wavelet transform and its advantages compared to Fourier transform," *Journal of Physical Sciences*, vol. 13, no. 4, pp. 121–134, 2009.

[23] S. Thakral and P. Manhas, "Image processing by using different types of discrete wavelet transform," in *Proc. of the 2nd ICAICR (Int. Conf. on Advanced Informatics and Computing Research)*, Shimla, Springer Singapore, vol. 955, 2019.

[24] C. Lutzweiler, S. Tzoumas, A. Rosenthal, V. Ntziachristos and D. Razansky, "High-throughput sparsity-based inversion scheme for optoacoustic tomography," *IEEE Transactions on Medical Imaging*, vol. 35, no. 2, pp. 674–684, 2016.

[25] M. Bitenc, D. S. Kieffer and K. Khoshelham, "Evaluation of wavelet denoising methods for small-scale joint roughness estimation using terrestrial laser scanning," *ISPRS (International Society for Photogrammetry and Remote Sensing) Annals of the Photogrammetry, Remote Sensing and Spatial Information Sciences*, vol. 2, no. 3W5, pp. 81–88, 2015.

[26] R. P. Medeiros and F. B. Costa, "A Wavelet-based transformer differential protection with differential current transformer saturation and cross-country fault detection," *IEEE Transactions on Power Delivery*, vol. 33, no. 2, pp. 789–799, 2018.